Reconfiguration of Langmuir Monolayers of Thermo-Responsive Hyperbranched Ionic Polymers with LCST Transition

*Paraskevi Flouda,[a] Alexandr V. Stryutsky,[b] Madeline L. Buxton,[a] Katarina M. Adstedt,[a] Daria Bukharina,[a] Valery V. Shevchenko,[b] and Vladimir V. Tsukruk[a]**

[a]School of Materials Science and Engineering, Georgia Institute of Technology, Atlanta, Georgia 30332, USA.

[b]Institute of Macromolecular Chemistry of the National Academy of Sciences of Ukraine, Kharkivske Shosse 48, Kyiv 02160, Ukraine.

*E-mail: vladimir@mse.gatech.edu

Abstract

Thermo-responsive ionic polymers have the ability to form adaptive and switchable morphologies, which may offer enhanced control in energy storage and catalytic applications. Current thermo-responsive polymers are composed of covalently attached thermo-responsive moieties, restricting their mobility and global dynamic response. Here, we report the synthesis and assembly at the water-air interface of symmetric and asymmetric amphiphilic thermo-responsive hyperbranched polymers with weakly ionically bound arms of amine-terminated poly(N-isopropylacrylamide) (PNIPAM) macro-cations. As we observe, symmetric branched polymers formed multimolecular nanosized micellar-assemblies, whereas corresponding asymmetric polymers formed large, interconnected worm-like aggregates. Dramatic changes in localized and large-scale chemical composition confirmed the reversible adsorption and desorption of the mobile PNIPAM macro-cations below and above the low critical solution temperature (LCST) and their non-uniform redistribution within polymer monolayer. Increasing the temperature above LCST led to the formation of large interconnected micellar aggregates because of the micelle-centered aggregation of the hydrophobized PNIPAM macro-cationic terminal chains at aqueous subphase. Overall, this work provides insights in the dynamic nature of the chemical composition of branched ionic polymers with weakly ionically bound thermo-responsive terminal chains and its effect on both morphology and surface chemistry at LCST transition.

Keywords: *hyperbranched ionic polymers, thermo-responsive ionic polymers, poly(N-isopropylacrylamide) (PNIPAM), Langmuir-Blodgett monolayers*

1. Introduction

Polymers bearing multifunctional ionizable groups in different configurations have emerged over the last decades due to their broad chemical structures, physicochemical properties, and ability to form various dynamically controlled morphologies depending on external stimuli such as ionic strength.[1,2] A variety of different morphologies has been reported including spherical micelles, vesicles, cylindrical micelles, star-like, and lamellar mesophases leading to unique properties and applications.[3, 4, 5, 6, 7] Specifically, multimolecular micellar-like morphologies play an important role in biomedical and industrial applications due to their potential as drug delivery systems and catalytic nanoreactors.[8, 9] On the other hand, elongated and interconnected ion-conductive morphologies with enhanced transport abilities are of interest in electronic and energy storage applications.[10]

The assembly of polymers with ionizable groups depends on the polymer architecture, terminal groups, and the ratio between hydrophobic and hydrophilic segments.[11] For example, spherical micellar structures with sizes of 100 – 500 nm were formed from star-shaped poly(ionic liquid)s (PILs) based on imidazolium/bis(trifluoromethane)sulfonimide with different lengths of the arms.[4] Similarly, the length of the alkyl chains of amphiphilic linear polymers composed of N-imidazole-3-propylmethacrylamide and alkyl (methyl and ethyl) chains controls the spontaneous polymer self-assembly in water and may lead to the formation of vesicles with much smaller sizes down to 60 nm.[3] Well-defined onion-like and ellipsoid-like nanoparticles of 50 nm across with internal subdomains of 5 nm were also observed to form from linear PILs containing 1,2,4-triazolium-based ionic liquid monomers (TILMs).[5]

As a way to control the polymer assembly and realize complex pre-programmed and responsive morphologies as triggered by low critical solution transition (LCST), thermo-responsive ionic polymers have been synthesized and investigated.[12] Typically, such polymers are linear random copolymer or block copolymers composed of covalently-connected thermo-responsive moieties and ionizable groups.[13, 14, 15, 16] For example, amphiphilic diblock copolymers of hydrophobic polyisobutylene (PIB) coupled with hydrophilic poly(2-ethyl-2-oxazoline) (PetOx) via imidazolium groups exhibited an LCST transition at 72 ºC – 90 ºC and formed supramolecular assemblies such as spherical or elongated micelles, and wormlike aggregates depending on the composition of the hydrophilic/hydrophobic segments.[17] As it has been shown, the variation of the block length ratio by shortening the PEtOx block while keeping the PIB block length constant

changes the geometric constrains for spherical micellar packing leading to a transition to cylindrical micellar morphologies.[17]

Only a handful of reports have focused on compact hyperbranched ionic thermo-responsive LCST polymers with different chemical compositions of terminal groups.[18, 19, 20, 21] For example, the synthesis of hyperbranched poly(3-ethyl-3-hydroxymethyloxetane) (PEHO) cores with inner polyionic imidazolium and outer thermo-responsive polyoxazoline (POx) shells has recently been reported.[18] The hyperbranched polymers formed micelles and demonstrated an LCST in an aqueous medium between 21 ºC and 93 ºC depending on their polarity and the hydrophilicity/hydrophobicity balance.[18] However, in these reports the thermo-responsive moieties were firmly covalently attached to the polymers restricting their mobility and dynamic response in solution.

In contrast, the synthesis and assembly of thermo-responsive LCST polymers composed of hydrophobic polyester cores and weakly ionically tethered PNIPAM terminal macro-cations were only recently reported.[19, 20, 21] The hyperbranched polymers with weakly-bonded thermo-responsive segments formed diverse unimolecular organized morphologies such as micelles, disk-like domains, and network ridge-like domains depending on the polymer composition and assembling conditions.[20, 21] Molecular dynamics simulations on these branched polymers containing sulfonate polyester cores, 16 alkyl arms, and 16 PNIPAM macro-cations suggested high mobility of weakly tethered terminal PNIPAM chains. Indeed, the ionically tethered macro-cation chains were able to desorb and dynamically hop between different anionic sulfonate sites of the polyester cores.[21]

Here, we report on the synthesis and assembly of novel amphiphilic branched polymers with weakly-bonded thermo-responsive terminal ionizable groups with symmetric and asymmetric peripheral hydrophobic/hydrophilic composition (**Scheme 1**). Symmetric hyperbranched polymers composed of carboxylate polyester cores with 16 hydrophobic n-octadecyl urethane groups and 16 hydrophilic PNIPAM macro-cations and asymmetric polymers composed of the same cores and 8 hydrophobic alkyl chains and 24 hydrophilic PNIPAM macro-cations were synthesized and studied (**Scheme 1**). The assembly of multimolecular micellar structures at the air-water interface was investigated below and above the LCST transition under different surface pressures. We observed that the symmetric hyperbranched polymers formed small micelles that

increased in size with pressure and eventually formed continuous networks, whereas the asymmetric hyperbranched polymers formed continuous networks even at low surface pressures. However, above the LCST temperature, both polymers formed large, interconnected domains because of the LCST transition of the PNIPAM macro-cations that leads to increased hydrophobicity. Finally, the localized chemical composition and properties of the assembled films were investigated using a unique combination of AFM-IR and Peak-Force Kelvin microscopy (PF-KPFM), scanning probe microscopy (SPM) modes to unravel the role of the mobile thermo-responsive macro-cations. It was revealed that terminal PNIPAM macro-cations are, in fact, able to reversibly dissociate from the anionic cores at LCST temperature resulting in dramatic reconfiguration not only the monolayer morphology, but also the distribution of surface chemistries and surface charges.

Scheme 1. Schematic representation (left) and chemical structures (right and bottom) of the symmetric (C16P16) and asymmetric (C8P24) thermo-responsive ionic polymers studied in this work

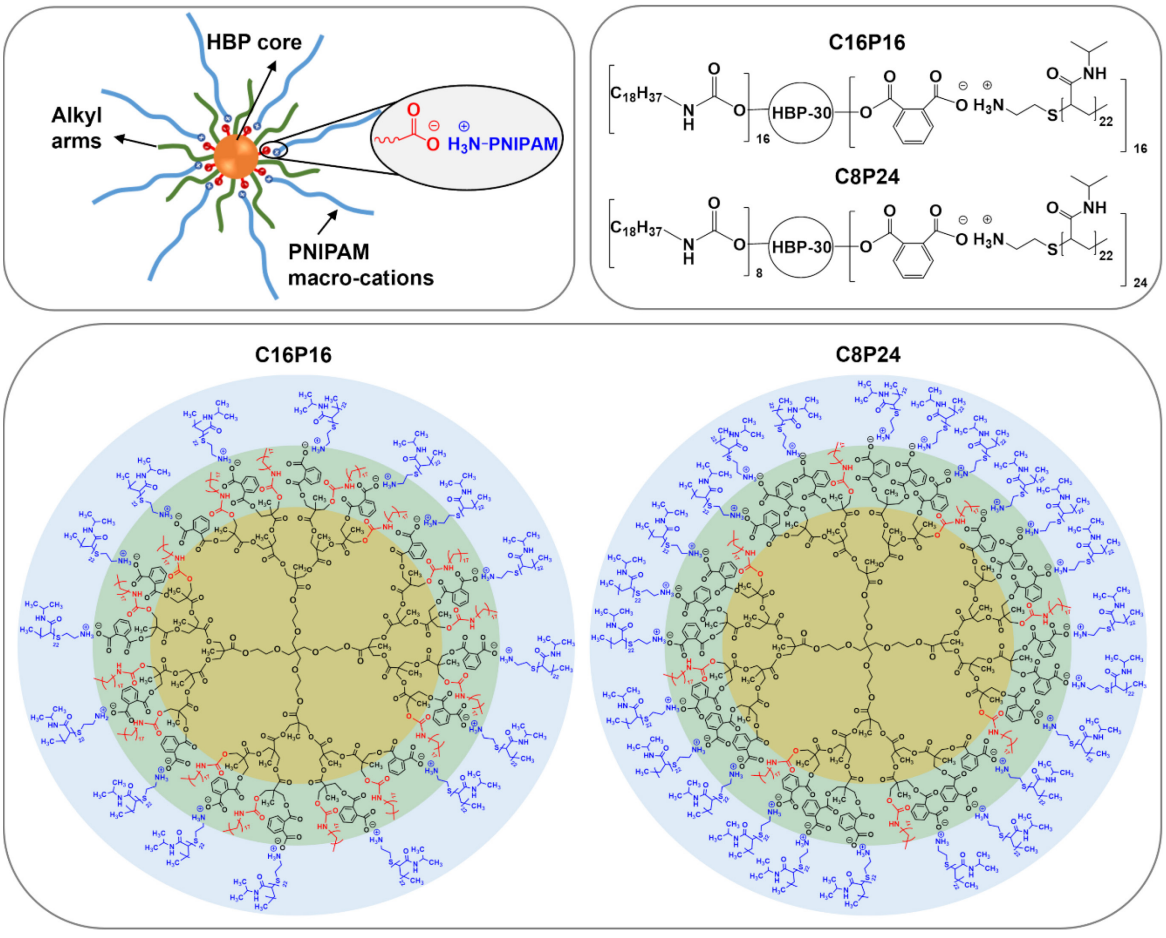

2. Methods

Synthesis of hyperbranched polymers. PNIPAM amine terminated (PNIPAM, M_n = 2500 g/ mol) was purchased from Sigma-Aldrich. Hyperbranched aliphatic polyester polyol (Boltron H30, Perstorp, M_w = 3500 g/mol) composed of 32 hydroxyl terminal groups in the outer shell was purified by precipitation of dimethyl formamide (DMF) solution in diethyl ether and drying at 25 – 30 ^oC under vacuum for 6h. Similarly, phthalic anhydride was purified by sublimation. All solvents, such as DMF, diethyl ether, and ethanol were dried and distilled before use. Ultrapure water (resistivity ≥ 18.2 MΩ·cm) was used for all experiments.

Synthesis of the hyperbranched thermo-responsive ionic polymers was conducted according to our previous report (Ref. 20) by partial blocking of the hydroxyl groups of the hyperbranched polyester polyol (HBP-OH) with n-octadecyl isocyanate, acylating the remaining hydroxyl groups with phthalic anhydride followed by neutralization of the carboxylate groups of the resultant oligomeric acids by the amino groups of PNIPAM (**Figure S1).** The ratio between the octadecyl tails and ionic groups was set as 1:1 (C16P16) and 1:3 (C8P24), respectively (see **Supporting Information** for more details). The synthesized polymers belong to a special category of branched polyelectrolytes with a substantial portion of their constitutional units composed of ionized end groups.[22] The hyperbranched polymers were dissolved in chloroform at a concentration of 20 mg/ml under stirring overnight at room temperature.

Langmuir-Blodgett (LB) films. The Langmuir isotherms and LB monolayers on piranha treated silicon wafers were obtained using a KSV 2000 minitrough with temperature controlled subphase. Solutions of hyperbranched polymers in ethanol at a concentration of 0.2 mg/ml were spread dropwise on the water surface and left undisturbed for 30 min to allow for solvent evaporation. Compression isotherms at different temperatures were obtained to the maximum pressure and the maximum trough area at a rate of 5 mm/min. LB monolayers on silicon wafers were deposited by vertical dipping at 1 mm/min at the preferred surface pressure.

Characterization. Fourier transform infrared (FT-IR) spectra of the polymer powders as tablets with KBr were collected using a Bruker Vertex 70 FTIR spectrophotometer within the 800 – 4000 cm^{-1} range with a resolution of 4 cm^{-1} and 200 scans. Proton nuclear magnetic resonance (^{1}H NMR) spectra were taken with Varian VXR-400 MHz spectrometer with DMSO-d_6 as the solvent. Molecular models were constructed using Chem3D 20.1.1(MM2 force field).[19]

Thermal properties were investigated by thermogravimetric analysis (TGA) and differential scanning calorimetry (DSC) using a TGA Q600 STD and a DSC Q200 (TA Instruments), respectively. Prior to thermal characterization all samples (~ 10 mg) were dried overnight under vacuum at 80 ºC. TGA was performed within the temperature range of 25 to 500 ºC at a heating rate of 10 ºC/min under nitrogen. DSC was conducted within the temperature range of – 50 to 150 ºC at a heating/cooling rate of 10 ºC/min under nitrogen. Two heating/cooling cycles were conducted and the curves from the second cycle were used to determine the glass transition temperature.

The LCST was determined by observing the transmittance of aqueous polymer solutions (0.2 mg/ml) at 500 nm using a Shimadzu UV-3600 Plus Spectrophotometer and heating/cooling the solutions with a rate of 1 ºC/min. The aqueous polymer solutions were prepared by adding the dissolved polymers in ethanol dropwise to water under stirring. Ethanol was evaporated under stirring for 48h and mixtures of hyperbranched polymers in water with a concentration of 0.5 mg/ml were obtained.

Zeta-potential and size of the hyperbranched polymers in water (0.2 mg/ml) were measured at three different temperatures (25 ºC, 38 ºC, and 50 ºC) with a Zetasizer Nano ZS (Malvern Instruments, at 633 nm, scattering angle of 173º) in polystyrene cuvettes. The average of three measurements was taken.

The morphology of the assemblies was characterized using atomic force microscopy (AFM) with a Bruker Dimension Icon microscope operated in soft tapping mode in air.[23] Scans with a resolution of 512 x 512 at a scan rate of 0.5 Hz were taken using AFM probes (HQ:XSC11/AI BS) with a spring constant of 1.1 – 5.6 N/m and a nominal tip radius of 8 nm. High-resolution images were taken using high-resolution AFM probes (MikroMasch, Hi'Res-C18/Cr-Au) with a nominal tip radius of 1 nm and a spring constant of 2.8 N/m.

Surface potential measurements were conducted using Peak-Force Kelvin probe force microscopy (PF-KPFM) mode. AFM probes (PFQNE-AL) specifically designed for PF-KPFM with a tip radius of 5 nm and a spring constant of 0.8 N/m were used. Images were collected with a resolution of 512 x 512, a scan rate of 0.5 Hz, and at a lift height of 100 nm.

Nanoscale characterization of surface chemical composition (AFM-IR) was performed using an Anasys NanoIR2 system operating with top-down illumination.[24] The AFM scans were taken

in contact mode using AFM probes (PR-EX-nIR2-10) with a tip radius of 40 nm and a spring constant of 0.07 N/m. While scanning, the samples were subjected to pulses from a tunable infrared source. Individual spectra were taken from 1400 to 1800 cm^{-1} with a resolution of 4 cm^{-1} at ten different locations on the micellar aggregates and ten locations on the surrounding area for comparative chemical composition analysis. Furthermore, chemical mappings of 5 μm x 5 μm were obtained at 1738 cm^{-1} with a resolution of 512 x 512 and a scan rate of 0.4 Hz.

Contact angle measurements were conducted using a KSV CAM101 system for 40 μl of water droplets. The measurements were taken within 10s of the water applications at three different locations of each specimen.

3. Results and discussion

Synthesis of thermo-responsive hyperbranched polymers. Symmetric and asymmetric amphiphilic hyperbranched polymers bearing carboxylate terminal groups and thermo-responsive PNIPAM macro-cations weakly bound to the negatively charged terminal groups of the hyperbranched cores were synthesized (**Scheme 1** and **Figure S1**). Specifically, the symmetric polymers (referred as C16P16) contained 16 hydrophobic n-octadecylurethane arms and 16 hydrophilic PNIPAM macro-cations, while the asymmetric (referred as C8P24) were composed of 8 hydrophobic arms and 24 PNIPAM macro-cations.

The chemical composition of the hyperbranched polymers was confirmed by FT-IR (**Figure 1**) and ^{1}H NMR (**Figure S2** and **Figure S3**). The two polymers had similar FT-IR spectra as they were composed of the same chemical moieties. Absorption bands corresponding to aliphatic fragments of the hyperbranched core, PNIPAM macro-cations, and octadecyl urethane chains were observed. These include bands for νC−H of CH_2 at 2876 cm^{-1}, 2932 cm^{-1}, 2974 cm^{-1}, δC−H of CH_2 and δC−H asymmetric of CH_3 at 1457 cm^{-1}, δC−H symmetric of CH_3 at 1367 cm^{-1}, 1387 cm^{-1}, and νC−H of CH_3 at 1090 − 1315 cm^{-1}.[21] Peaks associated with νC−O−C bonds (1000 − 1312 cm^{-1}) of ester fragments overlap with the νC−H of CH_3.[21, 25] Additional absorption peaks at 1717 − 1736 cm^{-1} were observed due to ester and carboxylate groups.[21, 25] Furthermore, the characteristic bands for the PNIPAM amide groups were apparent at ~1649 cm^{-1} and ~1543 cm^{-1} for νC=O amide I at and δN−H amide II, respectively.[21, 26] At higher wavenumbers, bands due to νC−H of aromatic rings at 3075 cm^{-1}, urethane groups, amide, and ammonium cations at 3100 –

3700 cm^{-1} were observed.[21, 26] Increasing the PNIPAM macro-cation content led to an increase in the intensity of the PNIPAM associated peaks such as the amide I and amide II peaks, as well as a decrease in the intensity of the C=O ester and carboxylate groups.

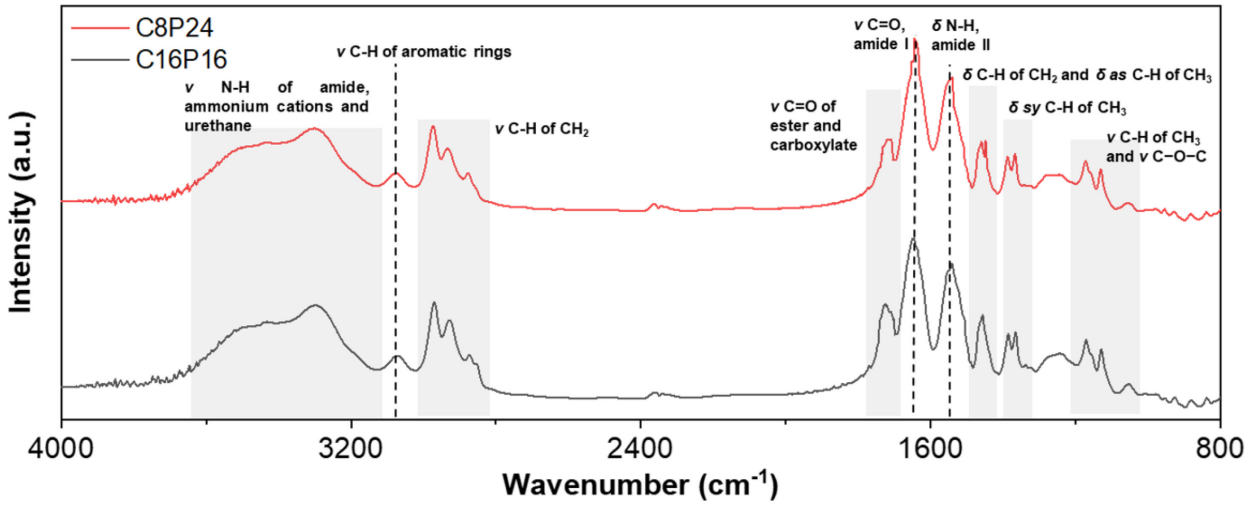

Figure 1. FT-IR spectra of the symmetric (C16P16) and asymmetric (C8P24) thermo-responsive ionic polymers with characteristic vibrational bands.

Overall, ^{1}H NMR spectra show the characteristic signals for the methyl and methylene groups of the hyperbranched cores, n-octadecylurethane arms, and PNIPAM chains in the range of 0.74 - 4.42 ppm (**Figure S2** and **Figure S3**). Furthermore, peaks of protons from tertiary carbon atoms of PNIPAM chains (1.97 - 1.98, 3.85 ppm) were observed. The signals in the ranges of 7.00 - 8.26 ppm and 8.76 - 8.77 ppm are attributed to the aromatic rings and amide groups, and ammonium cations of PNIPAM, respectively. The chemical structures and the neutralization degree of the hyperbranched polymers is confirmed by both the positions of the NMR peaks corresponding to characteristic groups and the ratios of the signal integral areas.

Thermal behavior. The hyperbranched polymers exhibited similar thermal stability, with a degradation temperature at 370 ºC and an onset at 181 ºC (defined as the 5 wt% degradation temperature) (**Figure S4a)**. DSC curves revealed glass transition temperatures at 97.2 ºC and 100.1 ºC for C16P16 and C8P24, respectively, with no signs of crystallization (**Figure S4b**). Increasing the number of PNIPAM macro-cations caused an increase in the T_g due to the higher T_g of the grafted PNIPAM entities.[27, 28] Overall, these values are significantly lower than the T_g values of linear high molecular weight PNIPAM containing polymers (110 – 140 ºC).[27, 28] The lower T_g

values are attributed to the hyperbranched polyester cores with glass transition in the range of 25 to 40 °C and the different glass transition mechanism for branched macromolecules which relies on the translational motion of the branches.[29, 30]

In aqueous solutions, both polymers exhibited a narrow LCST phase transition (defined as the temperature where transmittance decreases by 10%)[31] at 36.0 ± 0.2 °C for C16P16 and 34.2 ± 0.3 °C for C8P24, as shown in **Figure 2a-b** and **Table 1**. The LCST values of the synthesized polymers are relatively higher to the LCST of traditional linear PNIPAM homopolymers, ~ 32 °C.[32] The increased LCST temperatures are in agreement with previously reported hyperbranched polymers with PNIPAM components and are attributed to the Coulombic interactions between the anionic polyester cores and the PNIPAM macro-cations that can stabilize polymers at higher temperatures.[19, 33] Furthermore, the lower LCST of C8P24 compared to C16P16 is attributed to the increased density of the ionically tethered PNIPAM macro-cations that induce the coil-to-globule transition at low temperatures.[34]

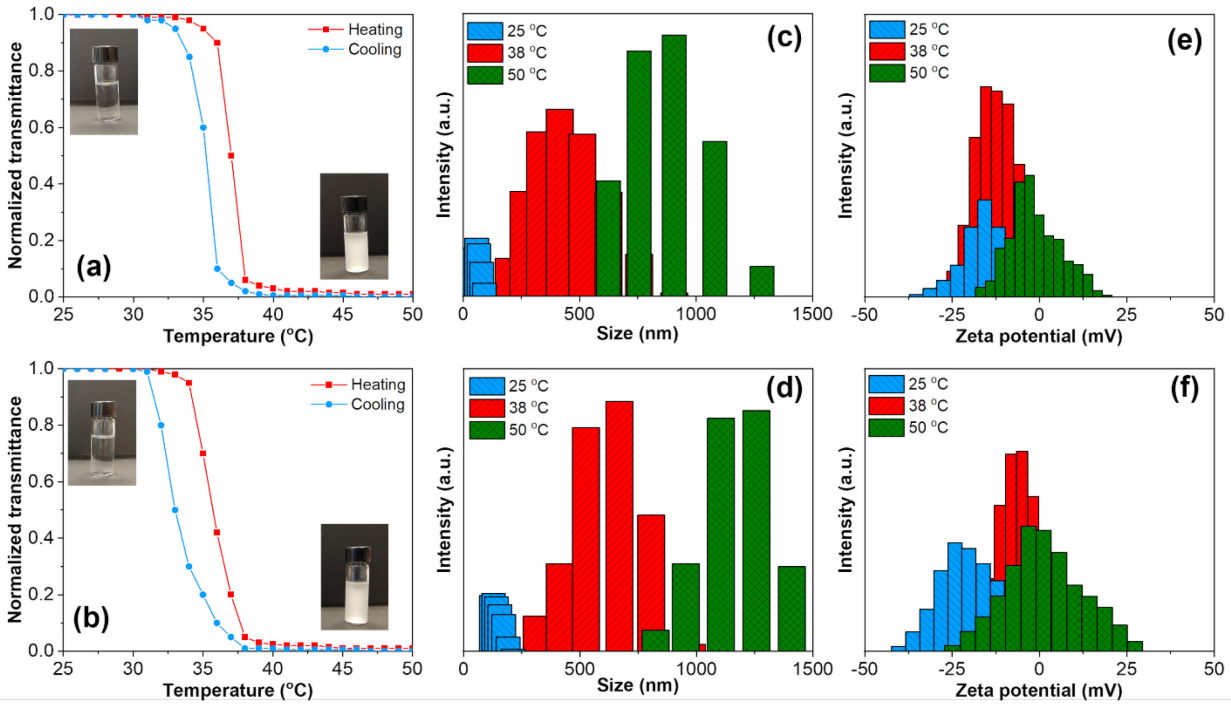

Figure 2. (a,b) Transmittance, (c,d) size, and (e,f) zeta potential vs. temperature for (a, c, e) C16P16 and (b, d, f) C8P24. Insets in panels (a) and (b) show optical images at 25 °C and 50 °C of the polymer aqueous solutions.

Upon cooling, a temperature hysteresis of 2.2 – 2.6 °C was observed for both polymers which is smaller compared to literature data for such polymers.[35] The narrow temperature hysteresis

indicates fast diffusion of water molecules inside the polymer assemblies upon cooling.[35] The larger hysteresis for C8P24 compared to C16P16 is indicative of diffusion limitations due to the higher density of the long PNIPAM macro-cations, collapsed above LCST, that strongly interact through hydrogen bonding interactions and lead to slower morphological tansitions.[35]

Table 1. Thermal properties of the ionic hyperbranched polymers.

Samples		25 °C		38 °C		50 °C	
	LCST (°C)	D_{DLS} (nm)	ζ-pot. (mV)	D_{DLS} (nm)	ζ-pot. (mV)	D_{DLS} (nm)	ζ-pot. (mV)
C16P16	36.0 ± 0.2	61 ± 21	-15.9 ± 1.2	404 ± 51	-12.2 ± 1.4	880 ± 79	2.9 ± 0.6
C8P24	34.2 ± 0.3	152 ± 30	-12.9 ± 1.1	671 ± 39	-9.4 ± 2.9	1260 ± 90	-1.8 ± 1.0

Additionally, the hyperbranched polymers showed a temperature-induced size change resulting from the LCST transition of PNIPAM arms (**Figure 2c-d** and **Table 1**). More specifically, C16P16 demonstrated average hydrodynamic diameters of 61 ± 21 nm and C8P24 exhibited much larger sizes of 152 ± 30 nm at 25 ºC. These values are comparable to micelle sizes of other symmetric and asymmetric amphiphilic hyperbranched ionic polymers with polyester cores.[20] Elevated temperatures promoted the formation of larger micelles due to the enhanced hydrophobicity of the terminal PNIPAM macro-cations.[20] The size of C16P16 micelles increased to 404 ± 51 nm at 38 ºC and 880 ± 79 nm at 50 ºC. Similarly, the size of C8P24 micelles increased to 671 ± 39 nm at 38 ºC and 1260 ± 90 at 50 ºC. Overall, the asymmetric polymer formed micelles with larger hydrodynamic diameters compared to symmetric macromolecules resulting from the higher density of the large PNIPAM macro-cations leading to aggregated particles, as will be discussed below.

Similarly, elevated temperatures promoted changes in the zeta potential of the ionic hyperbranched polymers (**Figure 2e-f** and **Table 1**). C16P16 showed an average zeta potential of -15.9 ± 1.2 mV at 25 ºC, which is comparable to other hyperbranched polymers bearing carboxylate terminal groups.[6, 21, 19] C8P24 possess a similar zeta potential of -12.9 ± 1.1 mV at the same conditions. The similar zeta potential values at 25 ºC for both polymers despite their different macro-cation densities indicate the screening of the core anionic carboxylate groups by the PNIPAM macro-cations. Furthermore, C16P16 exhibited a value of -12.2 ± 1.4 mV and -2.9 ± 0.6 mV at 38 ºC and 50 ºC, respectively (**Table 1**). Similarly, C8P24 had zeta potential values of

-9.4 ± 2.9 mV at 38 ºC and -1.8 ± 1.0 mV at 50 ºC. Above LCST, the PNIPAM macro-cations collapse and screen the negatively charged carboxylate cores.[20, 36] The increase in the zeta potential values causes a decrease in the stability of the polymers and possible uncontrolled aggregation.[37]

LB film morphology. At the water-air interphase, all branched polymers formed stable layers due to their amphiphilic nature. The hydrophobic polyester cores and alkyl arms prevent the dissolution in the aqueous subphase, while the hydrophilic PNIPAM macro-cations submerge in the aqueous phase.[20, 21]

The shape of the pressure-area isotherms for C16P16 and C8P24 is typical of materials with amphiphilic nature with the appearance of three common and characteristic phases of gas, liquid, and solid upon compression.[38, 39, 40] The isotherms for C8P24 shifted to a smaller surface area compared to C16P16, indicating the formation of more compact structures (**Figure 3**). The shift for C8P24 can be attributed to the increased density of the PNIPAM arms that may lead to enhanced hydrogen bonding and electrostatic interactions. These interactions can re-arrange the hyperbranched polymers to adapt more compact conformations and form aggregates reducing the surface area that they occupy.

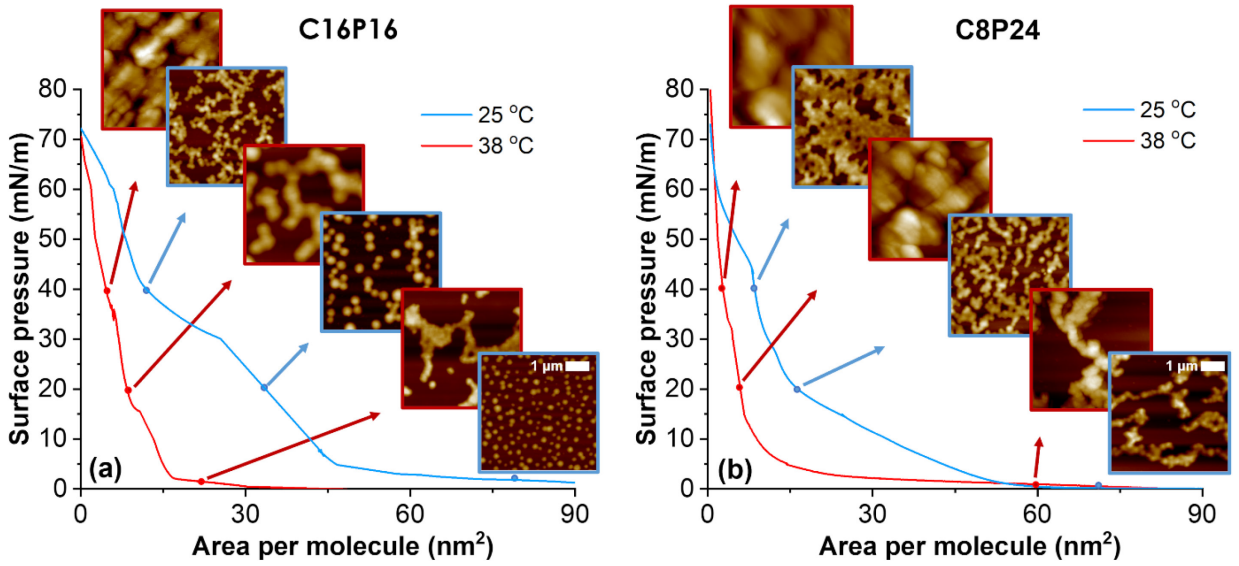

Figure 3. Langmuir isotherms for (a) C16P16 and (b) C8P24 polymers. Insets show AFM topography images. The Z axis is 45 nm for C16P16 and C8P24 at 0.3 mN/m at 38 ºC, 225 nm for C8P24 at 20 mN/m and 40 mN/m at 38 ºC, and 145 nm for all other images. The same scale bar of 1 µm applies to all AFM topography images.

At temperatures above LCST, the isotherms shifted significantly to smaller surface areas per molecule due to the increased hydrophobicity of the PNIPAM macro-cationic chains.[21] More specifically, the surface pressure started to increase below 45 – 55 nm^2 at 25 ºC, while at 38 ºC it started to rise below 15 – 10 nm^2 for both polymers. In all cases, the surface area rapidly increases below 5 – 10 nm^2 signifying the formation of solid monolayers.

Furthermore, a similar trend was observed upon monolayer decompression with all isotherms shifting towards smaller surface areas per molecule (**Figure S5**). This shift is attributed to the strong inter- and intra- molecular interactions and polymer chain entanglements that are formed during compression, which do not allow the PNIPAM macro-cations and alkyl chains to fully recover to their initial conformation.[41, 42] As a result, during the second compression cycle, the isotherms were shifted leading to the formation of more compacted morphology (**Figure S6)**.[41, 42]

AFM imaging reveals the morphological changes due to polymer peripheral composition, surface pressure and temperature assembly conditions (**Figure 3**, **Figure S7,** and **Figure S8**). Specifically, C16P16 films formed small collapsed micelles with a height of 28.4 ± 8.5 nm and a diameter of 208 ± 98 nm at 25 ºC and at a pressure of 0.3 mN/m. Dimensional analysis combined with molecular models shown in **Figure S9** suggests that these flattened micelles are multimolecular, composed of ~ 1060 molecules, indicating that the polymers aggregate fast in the presence of water. The formation of large aggregates at the water-air surface is attributed to strong electrostatic and hydrogen bonding interactions formed between the carboxylate polyester cores and the amine-terminated PNIPAM macro-cations. Upon compression, the micelles increase in size (height: 71.8 ± 12.9 nm, diameter: 472 ± 25 nm) and start to aggregate, ultimately forming larger chain-like aggregates at 40 mN/m.

Interestingly, asymmetric peripheral compositions led to the formation of various interconnected sub-micrometer irregular worm-like domains composed of micellar aggregates (**Figure 3** and **Figure S8**). The formation of irregular worm-like micelles despite the increased number of PNIPAM chains of the C8P24 indicates that the assembly is dominated by inter- and intra- molecular interactions such as electrostatic and hydrogen bonding interactions between the molecules rather than hydrophilic interactions, as explained in the discussion section. As expected, the layer compression led to the formation of large compact aggregated structures, confirming the observations made from the Langmuir isotherms analysis above.

Above LCST, the hyperbranched polymers exhibited strongly aggregated morphologies (**Figure 3**, **Figure S7,** and **Figure S8)**. C16P16 formed large domains composed of interconnected micelles with similar heights (60 – 90 nm) to the compressed micellar-like structures formed below LCST, resulting from core-core fusion between the micelles.[43] This morphological transition can be attributed to the increased hydrophobicity caused by the collapsed PNIPAM chains. Furthermore, increasing the content of PNIPAM macro-cations, promoted the formation of larger, merged domains. The formation of larger aggregates is thermodynamically favorable as it reduces the interfacial area between the hydrophobized polymers above LCST and the aqueous environment.[44]

Comparison of the micellar domain heights to the total film heights measured by AFM scratch tests reveal the existence of a continuous sublayer with thicknesses of 4 – 7 nm in all films formed below LCST (**Figure S10**). Surprisingly, above LCST, the continuous sublayer is absent as the hydrophobized polymers form large aggregates due to redistribution of material at interface.

The formation of a thin underlying nanolayer has been observed before for amphiphilic hyperbranched ionic polymers but its nature was not confirmed.[20, 21] It has been speculated that at a liquid phase the continuous sublayer is mainly composed of hydrophilic PNIPAM macro-cations, whereas at solid state the sublayer is formed from trapped hydrophobic and hydrophilic segments.[20, 21] These assumptions were made based on dimensional analysis of the molecules from molecular models.[20, 21] However, the true chemical composition of such sublayers has not been experimentally confirmed and thus has been considered here with novel AFM modes.

Changes in surface chemical composition. Here, unique AFM-IR measurements were conducted on samples prepared at 20 mN/m, as shown in **Figure 4, Figure 5,** and **Figure S11.** As known, AFM-IR allows for the chemical composition analysis at higher spatial resolutions (down to 10 nm) compared to conventional far-field IR spectroscopy revealing localized chemical composition of nano-sized domains.[45, 46] Specifically, AFM-IR mode can collect chemical maps and IR-spectra at selected locations via photothermal phenomenon at specific wavelengths showing the distribution of various chemical species.[45, 46]

AFM-IR mapping images of the C16P16 and C8P24 LB films assembled at 20 mN/m below and above LCST were collected at 1738 cm^{-1} wavenumber, which corresponds to vibrations of the ester and carboxylate groups from the hyperbranched cores (**Figure 4** and **Figure S11**).[21, 25] The

chemical maps showed high contrast indicating a variation of the surface chemistry of the films depending on the polymer peripheral composition and assembly conditions

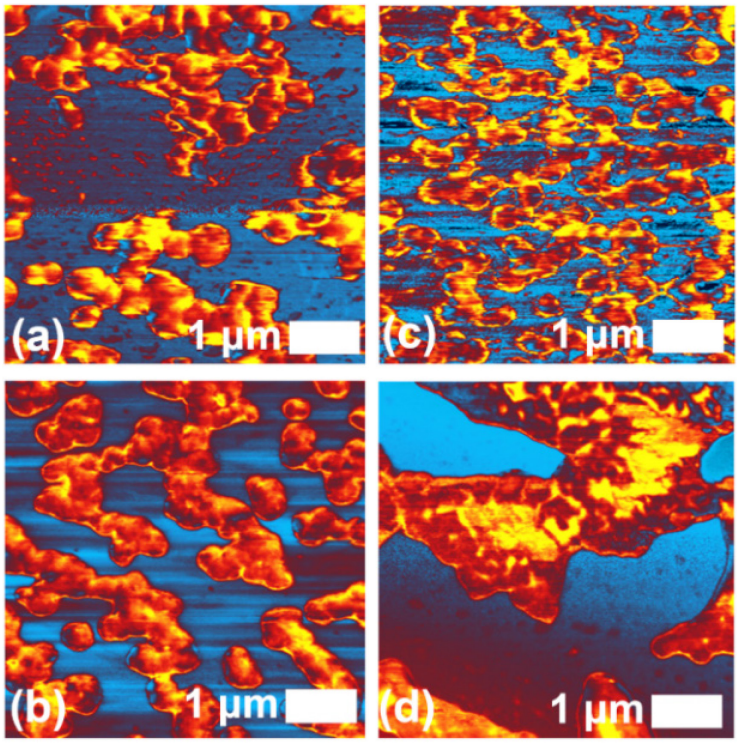

Figure 4. AFM-IR images at 1738 cm^{-1} and 20 mN/m for (a) C16P16 films at T = 25 ºC, (b) C16P16 films at T = 38 ºC, (c) C8P24 films at T = 25 ºC, and (d) C8P24 films at T = 38 ºC. Corresponding topography images are shown in **Figure S11**.

Specifically, localized IR-spectra with lateral resolution below 100 nm were collected from the aggregates and the domains in-between, as indicated by the small blue/red and black squares, respectively (**Figure 5**).[47] Overall, the LB films exhibited two strong bands at 1700 – 1760 cm^{-1} and 1435 – 1475 cm^{-1}, attributed to ester and carboxylate groups from the hyperbranched cores, and δC−H of CH_2 and δC−H asymmetric of CH_3, respectively.[21, 25] Furthermore, two weak bands were apparent above LCST at 1630 – 1680 cm^{-1} due to νC=O amide I and 1530 – 1580 cm^{-1} due to δN−H amide II bonds arising mainly from the presence of PNIPAM macrocations.[21, 26]

Below LCST, C16P16 and C8P24 monolayers showed the two strong bands for νC=O ester/carboxylate and δC-H vibrations at the domains in-between the aggregates. These bands indicate the expected presence of non-aggregated polyester cores at the domains in-between, as also shown in AFM-IR maps at 1738 cm^{-1} (**Figures 4**, **5**, and **S11**). Furthermore, weak amide bands

were observed in the domains in-between suggesting that a portion of the PNIPAM chains were bound to the non-aggregated polyester cores.

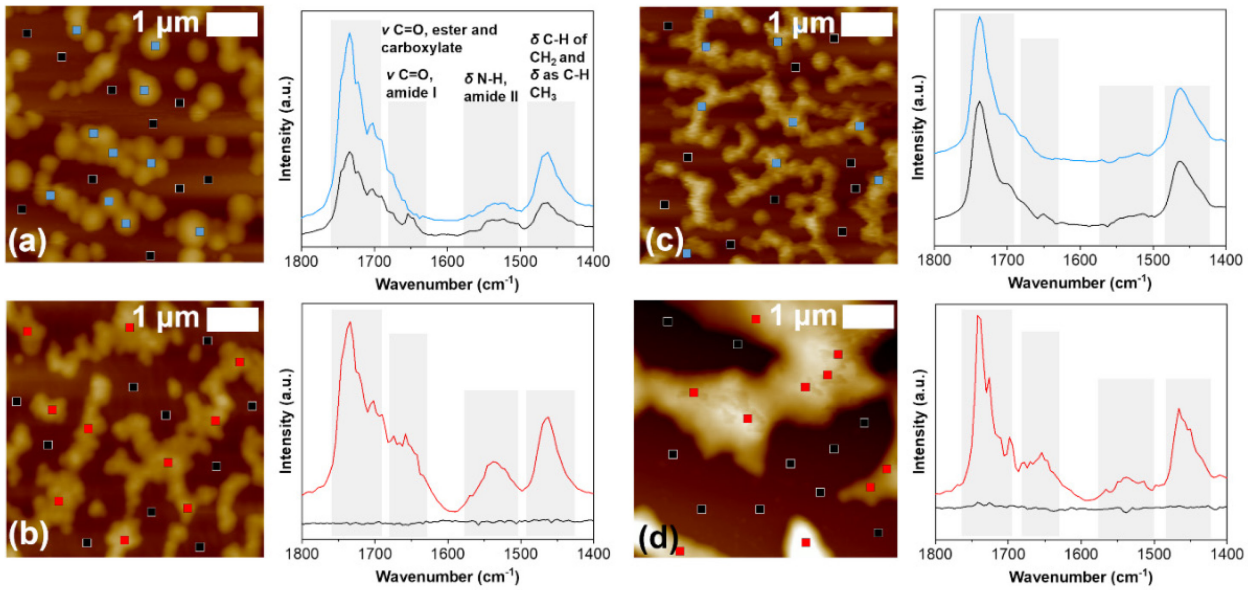

Figure 5. AFM topography images and average AFM-IR spectra from 10 measurements each for (a) C16P16 films at T = 25 ºC, (b) C16P16 films at T = 38 ºC, (c) C8P24 films at T = 25 ºC, and (d) C8P24 films at T = 38 ºC, assembled at 20 mN/m. The Z scale is 300 nm for panels (a), (b), (d), and 200 nm for panel (c).

At the aggregates, the two *ν*C=O ester/carboxylate and *δ*C-H bands were also observed. However, amide bands were absent, indicating that the surface of the micellar and worm-like aggregates is dominated by the hydrophobic polyester cores and alkyl chains of the hyperbranched polymers. Thus, we suggest that portion of the PNIPAM macro-cations is buried inside the micelles, while the rest are either weakly ionically bound to the polyester cores at the domains in-between the aggregates, or even dissociated in the aqueous medium.

For LB films deposited above the LCST temperature, IR-absorption bands were only observed at the aggregates, whereas the domains in-between did not exhibit any IR response. The results indicate that above LCST the polymers fully aggregate into large micellar-like domains due to their induced surface hydrophobization. Furthermore, the amide I and amide II bands were apparent at the micellar domains, suggesting that the PNIPAM dissociation was reversible, and dissociated hydrophobic PNIPAM macro-cations bounded again to the anionic polyester cores at the surface of the micellar assemblies.

To investigate the effect of varying the polymer peripheral composition on the reversible dissociation of the macro-cations, we deconvoluted the C=O bands (1600 – 1800 cm^{-1}) of the aggregates from the films formed above LCST (**Figure S12** and **Table S1**). Specifically, the bands were deconvoluted to individual peaks for free *ν*C=O ester and carboxylate bands at 1739 cm^{-1}, hydrogen bonded *ν*C=O ester and carboxylate bands at 1713 – 1720 cm^{-1}, and *ν*C=O amide I at 1657 – 1661 cm^{-1}.[48, 49, 50] Similar peak compositions were obtained for both C16P16 and C8P24. Despite the higher density of PNIPAM macro-cations in the C8P24 polymer, the C=O band was composed of 24.6 – 25.1 % amide I for both polymers, suggesting that the dissociation of PNIPAM chains may not be fully reversible for C8P24.

The changes in the global hydrophobicity of the LB films were also verified by water contact angle measurements (**Figure S13** and **Figure S14**). LB films formed below LCST demonstrated lower contact angles indicating predominant hydrophilicity of surfaces. Specifically, C16P16 showed a contact angle of 39.4 ± 0.6 º at a surface pressure of 0.3 mN/m, which increased to 57.5 ± 1.2 º and 60.3 ± 1.0 º at 20 and 40 mN/m, respectively. Above LCST, the surfaces turned to more hydrophobic with contact angles of 65.2 – 88.8º for C16P16. Similar behavior was observed for C8P24 with contact angles exceeding the 90º, indicating well developed global hydrophobicity.

Furthermore, we qualitatively investigated the surface charge distribution of the films using PF-KPFM, as shown in **Figure 6**.[21, 51]

As can be seen on these images, below LCST monolayers from both polymers showed high surface potential contrast. This high contrast arises from the formation of a dipole layer from the anionic carboxylate cores that are exposed at the surface of the micellar assemblies due to the dissociation of the PNIPAM macro-cations (**Figure 6a** and **6c**).[52] The surface potential contrast was more apparent for the case of C16P16 (~ 470 mV), whereas the contrast decreased for C8P24 to ~ 180 mV due to the formation of highly aggregated assemblies that leads to charge screening.[21] Above LCST, the surface potential images do not show significant surface potential differences (< 125 mV) within the films (**Figure 6b** and **6d**). The absence of the notable electrostatic contrast suggests that hydrophobic PNIPAM macro-cations collapse and screen the negatively charged polyester cores leading to overall charge neutralization of the surface of the aggregated micellar assemblies.

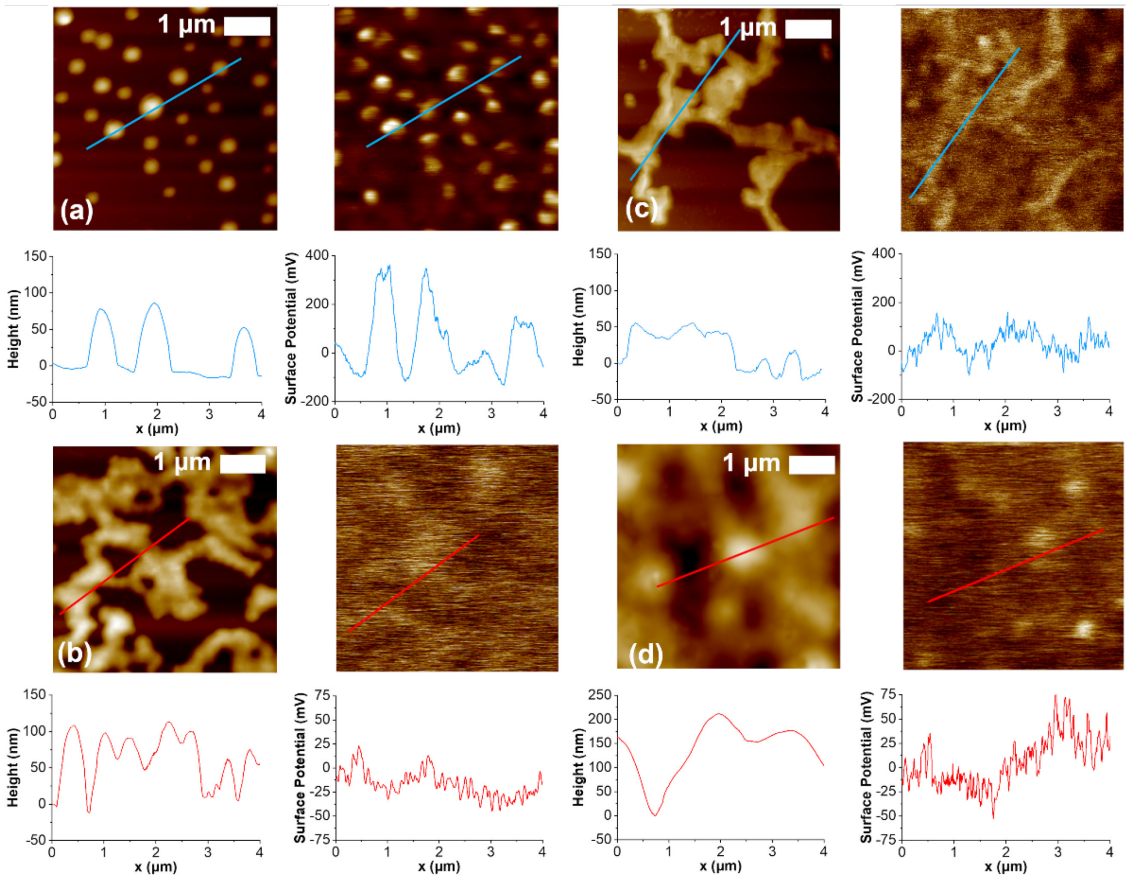

Figure 6. AFM topography and KPFM surface potential images for (a) C16P16 films at T = 25 ºC, (b) C16P16 films at T = 38 ºC, (c) C8P24 films at T = 25 ºC, (d) C8P24 films at T = 38 ºC, assembled at 20 mN/m. The Z-scale is 145 nm and 800 mV for panel (a), 200 nm and 140 mV for panel (b), 145 nm and 500 mV for panel (c), and 250 nm and 200 mV for panel (d).

These surface potential changes are in agreements with the ζ-potential and AFM-IR measurements that show a decrease in the absolute ζ-potential values and the appearance of amide I and II bands at the micellar aggregates. Decreased ζ-potential values suggest screening of the negatively charged cores and the appearance of the amide bands confirms that surface charge screening is caused by the collapsed PNIPAM macro-cations at the surface of the micellar aggregates leading to charge neutralization.

3. General discussion and conclusions

As we observed, the amphiphilic nature of the synthesized branched polymers facilitates the formation of stable layers at the water-air interphase which undergoes significant reconfiguration at LCST. Furthermore, the presence of the mobile terminal PNIPAM macro-cations leads to the

formation of a variety of morphologies with different surface chemistries under different assembly conditions. LB assemblies of the symmetric and asymmetric polymers demonstrated large micellar morphologies composed of >1000 molecules. This is in contrast with prior observations on hyperbranched polymers containing < 16 PNIPAM macro-cations per molecule, where unimolecular assemblies were observed.[20, 21] We suggest that the increased PNIPAM density leads to strong electrostatic and hydrogen bonding interactions between the anionic polyester cores with the PNIPAM macro-cations, and the polyester and alkyl chain ester bonds with the PNIPAM amide bonds, and results in the formation of the micellar assemblies.

Overall, the hyperbranched polymers synthesized in this study exhibited similar LCST temperatures with other linear and hyperbranched polymers containing PNIPAM from the literature.[19] Furthermore, varying the hydrophobic/hydrophilic ratio by varying the alkyl chain to PNIPAM ratio allowed us to create a unique variety of different morphologies and sizes compared to prior reports.[17, 18, 19] Finally, despite the formation of significantly larger polymer assemblies compared to the literature,[17, 18, 19] our polymers were still able to exhibit morphological changes with temperature, as a result of the dynamic, weakly ionically bound PNIPAM macro-cationic arms capable of dissociation and hopping between the anionic terminal sites of the polyester cores.[21]

Yet, the changes in the surface chemistry of large multimolecular assemblies of such polymers caused by the dynamic response of weakly ionically bound PNIPAM macro-cations had not been experimentally confirmed. In this study, the utilization of AFM-IR mode confirms the dynamic nature of weakly ionically bound PNIPAM macro-cations and their role in the reconfiguration of localized surface chemical composition of the monolayers at LCST. Specifically, it was confirmed that below LCST PNIPAM macro-cations are either buried inside the micellar aggregates or dissociated in the aqueous medium. Increasing the temperature above LCST, the PNIPAM macro-cationic chains were able to bound back to the anionic polyester cores at the surface of the micelles and simultaneously complete aggregation of the molecules took place due to the hydrophobization of the mobile PNIPAM chains. These results represent the first chemical confirmation of the local and global response of micellar aggregation with weakly ionically bound PNIPAM macro-cations at LCST.

Finally, **Table 2** compares the behavior of our LB assemblies against other multimolecular micellar assemblies of thermo-responsive LCST polymers. Specifically, we compare thermo-

responsive linear polymers, star block-co-polymers and hyperbranched polymers such as polyisobutylene (PIB) coupled with hydrophilic poly(2-ethyl-2-oxazoline) (PetOx) (PIB−IL−$PEtO_x$), poly(3-ethyl-3-hydroxymethyloxetane) (PEHO) cores coupled with polyionic imidazolium and thermo-responsive polyoxazoline (POx) shells (PEHO-IL-$P(EtO_x/nPrO_x)_y$), and linear (L-CA- 50% PNIPAM) and hyperbranched polymers (HBP-CA- 50% PNIPAM) containing 50 % of PNIPAM macro-cations and polyesters.[17, 18, 19]

Table 2. Multimolecular thermo-responsive polymer assemblies.

Polymer (conditions)	LCST (°C)	Below LCST		Above LCST		Ref.
		Shape	Size (nm)	Shape	Size (nm)	
PIB−IL−$PEtO_x$, star block copolymers	83 – 90	Micelles	Diameter: 25 – 40	-	-	17
PEHO-IL-$P(EtO_x/nPrOx)_y$, hyperbranched polymers	43 – 60	Micelles	Diameter: 20 – 28	-	-	18
L-CA-50 % PNIPAM, linear polymers	33.3 ± 0.2	Micelles	Diameter: 235 ± 60	Micellar aggregates	Length: 420 ± 120	19
HBP-CA-50% PNIPAM, hyperbranched polymers	34.7 ± 0.2	Micelles	Diameter: 172 ± 57	Vesicles	Diameter: 720 ± 330	19
C16P16, hyperbranched polymers (Surface pressure of 0.3 mN/m)	36.0 ± 0.2	Micelles	Height: 28.4 ± 8.5 and diameter: 208 ± 98	Network-like aggregates	Length: >1000	This work
C24P24, hyperbranched polymers (Surface pressure of 0.3 mN/m)	34.2 ± 0.3	Network-like aggregates	Length: > 500	Network-like aggregates	Length: >1000	This work

Based on the morphological and surface compositional analysis discussed above, we propose a molecular model for the molecular organization of the micellar-assemblies and tehir reorganization at LCST (**Figure 7**). Below LCST, both polymers form multimolecular assemblies with PNIPAM macro-cations either buried inside the micelles or dissociated in the aqueous medium. Simultaneously, non-aggregated molecules spread at the air-water interface, with the hydrophilic PNIPAM macro-cations spreading under water while hydrophobic carboxylate polyester cores and alkyl chains forming more compact assemblies above the PNIPAM chains. Above LCST, the hydrophobic molecules have formed large aggregates with the desorbed PNIPAM macro-cations preferentially bounded to the surface of the micellar-assemblies due to their LCST induced hydrophobicity. Compression favored the formation of large interconnected micellar-like domains with the molecules been closely packed.

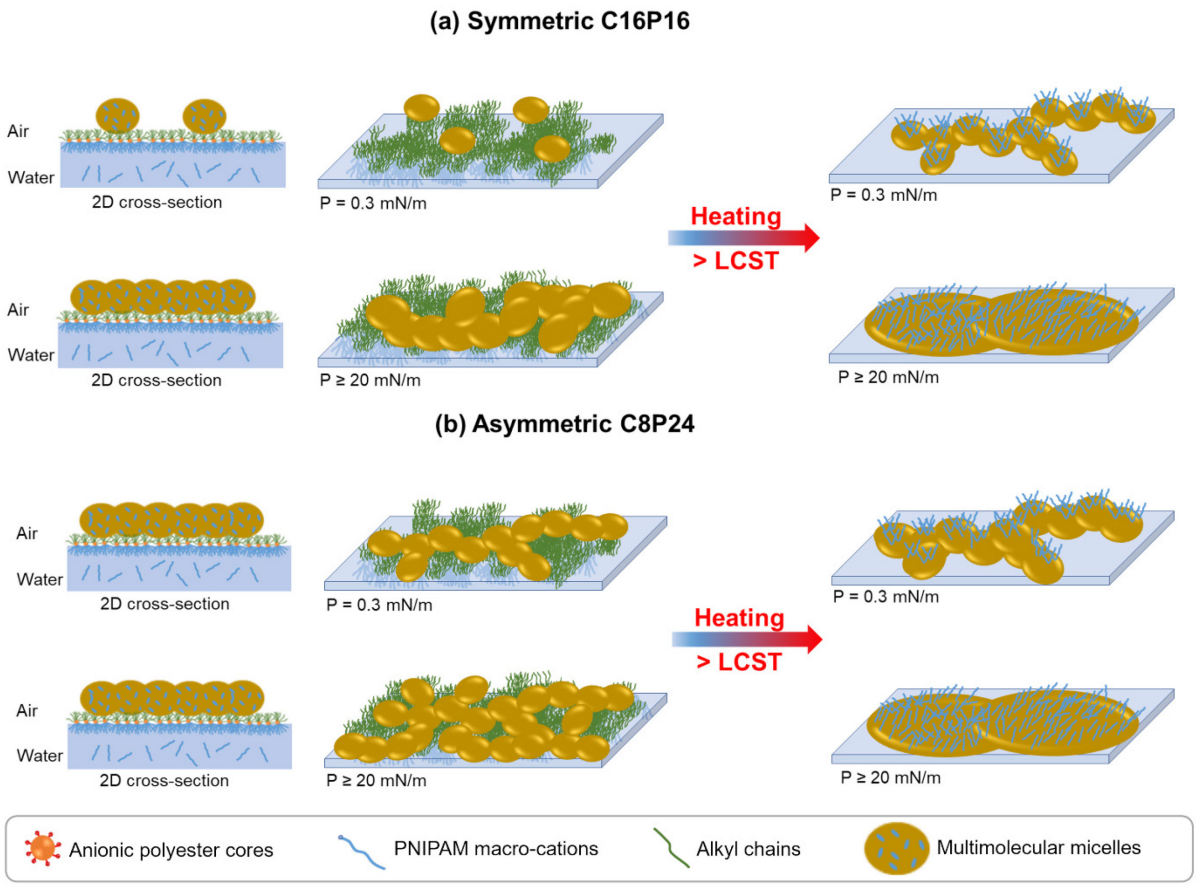

Figure 7. Schematic of the assembly of C16P16 and C8P24 branched polymers at the air-water interface at LCST transition, below (25 ºC) and above (38 ºC) at different surface pressures.

In conclusion, we investigated the assembly behavior and phase transformation of hyperbranched polymers with weakly ionically bound PNIPAM macro-cationic arms with varying balance of the hydrophobic/hydrophilic interactions. Notably, the dynamic nature of the thermo-responsive macro-cations and its effect on the surface chemistry of large multimolecular micellar assemblies was confirmed for the first time. The complex stimuli-responsive morphologies and surface chemistries of the hyperbranched thermo-responsive ionic polymers may have implications in energy storage and catalysis applications.

ASSOCIATED CONTENT

Supporting Information. Supporting Information is available free of charge at https://pubs.acs.org/doi/xx.xxxx.

AUTHOR INFORMATION

Corresponding author

Vladimir V. Tsukruk - School of Materials Science and Engineering, Georgia Institute of Technology, Atlanta, Georgia 30332, USA.

E-mail: vladimir@mse.gatech.edu

Author Contributions

The manuscript was written through contributions of all authors. All authors have given approval to the final version of the manuscript.

Funding Sources

This study is supported by the National Science Foundation DMR 2001968 and Air Force Research Laboratory grant FA8650-D-16-54 (AMF-IR measurements).

Notes

There are no conflicts to declare.

References

[1] Zhang, S.-Y.; Zhuang, Q.; Zhang, M.; Wang, H.; Gao, Z.; Sun, J.-K.; Yuan, J. Poly(Ionic Liquid) Composites. *Chem. Soc. Rev.* **2020,** *49*,1726-1755.

[2] Banerjee, P.; Anas, M.; Jana, S.; Mandal, T. K. Recent Developments in Stimuli-Responsive Poly(Ionic Liquid)s. *J. Polym. Res.* **2020**, *27*, 1-23.

[3] Manojkumar, K.; Mecerreyes, D.; Taton, D.; Gnanou, Y.; Vijayakrishna, K. Self-Assembly of Poly(Ionic Liquid) (Pil)-Based Amphiphilic Homopolymers into Vesicles and Supramolecular Structures with Dyes and Silver Nanoparticles. *Polym. Chem.* **2017**, *8*, 3497-3503.

[4] Erwin, A. J.; Lee, H.; Ge, S.; Zhao, S.; Korolovych, V. F.; He, H.; Matyjaszewski, K.; Sokolov, A. P.; Tsukruk, V. V. Viscoelastic Properties and Ion Dynamics in Star-Shaped Polymerized Ionic Liquids. *Eur. Polym. J.* **2018**, *109*, 326-335.

[5] Zhang, W.; Kochovski, Z.; Lu, Y.; Schmidt, B. V. K. J.; Antonietti, M.; Yuan, J. Internal Morphology-Controllable Self-Assembly in Poly(Ionic Liquid) Nanoparticles. *ACS Nano* **2016,** *10*, 7731-7737.

[6] Korolovych, V. F.; Ledin, P. A.; Stryutsky, A.; Shevchenko, V. V.; Sobko, O.; Xu, W.; Bulavin, L. A.; Tsukruk, V. V. Assembly of Amphiphilic Hyperbranched Polymeric Ionic Liquids in Aqueous Media at Different pH and Ionic Strength. *Macromolecules* **2016**, *49*, 8697−8710.

[7] Korolovych, V. F.; Erwin, A. J.; Stryutsky, A.; Mikan, E. K.; Shevchenko, V. V.; Tsukruk, V. V. Self-Assembly of Hyperbranched Protic Poly(ionic liquid)s with Variable Peripheral Amphiphilicity. *Bull. Chem. Soc. Jpn.* **2017**, *90*, 919−923.

[8] Yuan, Z.; Wang, J.; Wang, Y.; Zhong, Y.; Zhang, X.; Li, L.; Wang, J.; Lincoln, S. F.; Guo, X. Redox-Controlled Voltage Responsive Micelles Assembled by Noncovalently Grafted Polymers for Controlled Drug Release. *Macromolecules* **2019**, *52*, 1400-1407.

[9] Qu, P.; Kuepfert, M.; Ahmed, E.; Liu, F.; Weck, M. Cross-Linked Polymeric Micelles as Catalytic Nanoreactors. *Eur. J. Inorg. Chem.* **2021**, 1420-1427.

[10] Muthukumar, M. Theory of Ionic Conductivity with Morphological Control in Polymers. *ACS Macro Lett.* **2021**, *10*, 958-964.

[11] Xu, W.; Ledin, P. A.; Shevchenko, V. V.; Tsukruk, V. V. Architecture, Assembly, and Emerging Applications of Branched Functional Polyelectrolytes and Poly(Ionic Liquid)s. *ACS Appl. Mater. Interfaces* **2015**, *7*, 12570-12596.

[12] Kohno, Y.; Saita, S.; Men, Y.; Yuan, J.; Ohno, H. Thermoresponsive Polyelectrolytes Derived from Ionic Liquids. *Polym. Chem*. **2015**, *6*, 2163−2178.

[13] Men, Y.; Drechsler, M.; Yuan, J. Double-Stimuli-Responsive Spherical Polymer Brushes with a Poly(ionic liquid) Core and a Thermoresponsive Shell. *Macromol. Rapid Commun*. **2013**, *34*, 1721−1727.

[14] Nakabayashi, K.; Sato, Y.; Isawa, Y.; Lo, C.-T.; Mori, H. Ionic Conductivity and Assembled Structures of Imidazolium Salt-Based Block Copolymers with Thermoresponsive Segments. *Polymers* **2017,** *9*, 1-16.

[15] Luo, G.; Guo, Y.; Liu, C.; Han, G.; Ma, X.; Zhang, W. What Will Happen When Thermoresponsive Poly(N-Isopropylacrylamide) Is Tethered on Poly(Ionic Liquid)s. *RSC Adv.* **2019,** *9*, 12936-12943.

[16] Soll, S.; Antonietti, M.; Yuan, J. Double Stimuli-Responsive Copolymer Stabilizers for Multiwalled Carbon Nanotubes. *ACS Macro Lett*. **2012**, *1*, 84−87.

[17] Kerscher, B.; Trötschler, T. M.; Pásztói, B.; Gröer, S.; Szabó, Á.; Iván, B.; Mülhaupt, R. Thermoresponsive Polymer Ionic Liquids and Nanostructured Hydrogels Based Upon Amphiphilic Polyisobutylene-B-Poly(2-Ethyl-2-Oxazoline) Diblock Copolymers. *Macromolecules* **2019**, *52*, 3306-3318.

[18] Wiedmann, S.; Luitz, M.; Kerscher, B.; Lutz, J.-F.; Mülhaupt, R. Programmable Thermoresponsive Micelle-Inspired Polymer Ionic Liquids as Molecular Shuttles for Anionic Payloads. *Macromolecules* **2019,** *52*, 9672-9681.

[19] Korolovych, V. F.; Erwin, A.; Stryutsky, A.; Lee, H.; Heller, W. T.; Shevchenko, V. V.; Bulavin, L. A.; Tsukruk, V. V. Thermally Responsive Hyperbranched Poly(ionic liquid)s: Assembly and Phase Transformations. *Macromolecules* **2018**, *51*, 4923−4937.

[20] Lee, H.; Stryutsky, A. V.; Korolovych, V. F.; Mikan, E.; Shevchenko, V. V.; Tsukruk, V. V. Transformations of Thermosensitive Hyperbranched Poly(Ionic Liquid)S Monolayers. *Langmuir* **2019,** *35*, 11809-11820.

[21] Lee, H.; Stryutsky, A.; Mahmood, A.-U.; Singh, A.; Shevchenko, V. V.; Yingling, Y. G.; Tsukruk, V. V. Weakly Ionically Bound Thermosensitive Hyperbranched Polymers. *Langmuir* **2021,** *37*, 2913-2927.

[22] Hess, M.; Jones, R. G.; Kahovec, J.; Kitayama, T.; Kratochvil, P.; Kubisa, P.; Mormann, W.; Stepto, R. F. T.; Tabak, D.; Vohlidal, J.; Wilks, E. S. Terminology of Polymers Containing Ionizable or Ionic Groups and of Polymers Containing Ions. *Pure Appl. Chem*. **2006**, *78*, 2067−2074.

[23] McConney, M. E.; Singamaneni, S.; Tsukruk, V. V. Probing Soft Matter with the Atomic Force Microscopies: Imaging and Force Spectroscopy. *Polym. Rev*. **2010**, *50*, 235–286.

[24] Dazzi, A.; Prater, C. B. AFM-IR: Technology and Applications in Nanoscale Infrared Spectroscopy and Chemical Imaging. *Chem. Rev*. **2017**, *117*, 5146– 5173.

[25] Jena, K. K.; Raju, K. V. S. N.; Prathab, B.; Aminabhavi, T. M. Hyperbranched Polyesters: Synthesis, Characterization, and Molecular Simulations. *J. Phys. Chem. B* **2007,** *111*, 8801-8811.

[26] Futscher, M. H.; Philipp, M.; Müller-Buschbaum, P.; Schulte, A. The Role of Backbone Hydration of Poly(N-Isopropyl Acrylamide) across the Volume Phase Transition Compared to Its Monomer. *Sci. Rep.* **2017,** *7*, 1-10

[27] Lizundia, E.; Meaurio, E.; Laza, J. M.; Vilas, J. L.; Isidro, L. L. Study of the chain microstructure effects on the resulting thermal properties of poly(L-lactide)/poly(N-isopropylacrylamide) biomedical materials. *Mater. Sci. Eng., C* **2015**, *50*, 97−106.

[28] Biswas, C. S.; Patel, V. K.; Vishwakarma, N. K.; Tiwari, V. K.; Maiti, B.; Maiti, P.; Kamigaito, M.; Okamoto, Y.; Ray, B. Effects of Tacticity and Molecular Weight of Poly(N-isopropylacrylamide) on Its Glass Transition Temperature. *Macromolecules* **2011**, *44*, 5822− 5824.

[29] Dumitrascu, A.; Sarkar, A.; Chai, J.; Zhang, T.; Bubeck, R. A.; Howell, B. A.; Smith, P. B. Thermal Properties of Hyperbranched Polyesters. *J. Therm. Anal. Calorim*. **2018**, *131*, 273−280.

[30] Žagar, E.; Huskic, M.; Grdadolnik, J.; Z˘igon, M.; Zupancič -Valant, A. Effect of Annealing on the Rheological and Thermal Properties of Aliphatic Hyperbranched Polyester Based on 2,2-bis(methylol)propionic Acid. *Macromolecules* **2005**, *38*, 3933−3942.

[31] Boutris, C.; Chatzi, E. G.; Kiparissides, C. Characterization of the LCST Behaviour of Aqueous Poly(N-isopropylacrylamide) Solutions by Thermal and Cloud Point Techniques. *Polymer* **1997**, *38*, 2567−2570.

[32] Halperin, A.; Kröger, M.; Winnik, F. M. Poly(N-isopropylacrylamide) Phase Diagrams: Fifty Years of Research. *Angew. Chem., Int. Ed*. **2015**, *54*, 15342−15367.

[33] Lapworth, J. W.; Hatton, P. V.; Rimmer, S. Thermally Responsive Gels Formed from Highly Branched Poly(N-isopropyl acrylamide)s with Either Carboxylic Acid or Trihistidine End Groups. *RCS Adv*. **2013**, *3*, 18107−18114.

[34] Weng, Y.; Ding, Y.; Zhang, G. Microcalorimetric Investigation on the Lower Critical Solution Temperature Behavior of NIsopropycrylamide-co-Acrylic Acid Copolymer in Aqueous Solution. *J. Phys. Chem. B* **2006**, *110*, 11813−11817.

[35] Blackman, L. D.; Wright, D. B.; Robin, M. P.; Gibson, M. I.; O'Reilly, R. K. Effect of Micellization on the Thermoresponsive Behavior of Polymeric Assemblies. *ACS Macro Lett*. **2015**, *4*, 1210−1214.

[36] Karjalainen, E.; Chenna, N.; Laurinmaki, P.; Butcher, S. J.;¨Tenhu, H. Diblock Copolymers Consisting of a Polymerized Ionic Liquid and Poly(N-isopropylacrylamide). Effects of PNIPAM Block Length and Counter Ion on Self-Assembling and Thermal Properties. *Polym. Chem.* **2013**, *4*, 1014−1024.

[37] Freitas, C.; Müller, H. R. Effect of light and temperature on zeta potential and physical stability in solid lipid nanoparticle (SLN) dispersions. *Int. J. Pharm.* **1998**, *168*, 221−229.

[38] Zhai, X.; Peleshanko, S.; Klimenko, N. S.; Genson, K. L.; Vaknin, D.; Vortman, M. Y.; Shevchenko, V. V.; Tsukruk, V. V. Amphiphilic Dendritic Molecules: Hyperbranched Polyesters with Alkyl-terminated Branches. *Macromolecules* **2003**, *36*, 3101−3110.

[39] de Viguerie, L.; Keller, R.; Jonas, U.; Berger, R.; Clark, C. G.; Klein, C. O.; Geue, T.; Müllen, K.; Butt, H.-J.; Vlassopoulos, D. Effect of the Molecular Structure on the Hierarchical Self-Assembly of Semifluorinated Alkanes at the Air/Water Interface. *Langmuir* **2011,** *27*, 8776-8786.

[40] Genson, K. L.; Holzmueller, J.; Jiang, C.; Xu, J.; Gibson, J. D.; Zubarev, E. R.; Tsukruk, V. V. Langmuir−Blodgett Monolayers of Gold Nanoparticles with Amphiphilic Shells from V-Shaped Binary Polymer Arms. *Langmuir* **2006,** *22*, 7011-7015.

[41] Joncheray, T. J.; Denoncourt, K. M.; Meier, M. A. R.; Schubert, U. S.; Duran, R. S. Two-Dimensional Self-Assembly of Linear Poly(ethylene oxide)-b-poly(ε-caprolactone) Copolymers at the Air− Water Interface. *Langmuir* **2007**, 23, 2423−2429.

[42] Li, Z.; Ma, X.; Guan, X.; Qiang, X.; Zang, D.; Chen, F. Aggregation behavior of star-shaped fluoropolymers containing polyhedral oligomeric silsesquioxane (POSS) at the air-water interface. *Colloid Polym. Sci*. **2017**, 295, 157−170.

[43] Wang, L.; Wang, Y.; Miao, H.; Chen, D. Self-Assembly of Polymeric Micelles into Complex but Regular Superstructures Based on Highly Controllable Core–Core Fusion between the Micelles. *Soft Matter* **2016**, *12*, 4891-4895.

[44] Strandman, S.; Hietala, S.; Aseyev, V.; Koli, B.; Butcher, S. J.; Tenhu, H. Supramolecular Assemblies of Amphiphilic PMMA-Block-PAA Stars in aqueous Solutions. *Polymer* **2006**, *47*, 6524-6535.

[45] Dazzi, A.; Prater, C. B.; Hu, Q.; Chase, D. B.; Rabolt, J. F.; Marcott, C. Afm–Ir: Combining Atomic Force Microscopy and Infrared Spectroscopy for Nanoscale Chemical Characterization. *Appl. Spectrosc*. **2012**, *66*, 1365-1384.

[46] Schwartz, J. J.; Jakob, D. S.; Centrone, A. A Guide to Nanoscale Ir Spectroscopy: Resonance Enhanced Transduction in Contact and Tapping Mode AFM-IR. *Chem. Soc. Rev.* **2022**., *51*, 5248-5267.

[47] Ruggeri, F. S.; Vieweg, S.; Cendrowska, U.; Longo, G.; Chiki, A.; Lashuel, H. A.; Dietler, G. Nanoscale Studies Link Amyloid Maturity with Polyglutamine Diseases Onset. *Sci. Rep.* **2016**, 1-11.

[48] Žagar, E.; Grdadolnik, J. An Infrared Spectroscopic Study of H-Bond Network in Hyperbranched Polyester Polyol. *J. Mol. Struct.* **2003**, *658*, 143-152.

[49] Jena, K. K.; Chattopadhyay, D. K.; Raju, K. V. S. N. Synthesis and Characterization of Hyperbranched Polyurethane–Urea Coatings. *Eur. Polym. J.* **2007**, *43*, 1825-1837.

[50] Florian, P.; Jena, K. K.; Allauddin, S.; Narayan, R.; Raju, K. V. S. N. Preparation and Characterization of Waterborne Hyperbranched Polyurethane-Urea and Their Hybrid Coatings. *Ind. Eng. Chem. Res.* **2010**, *49*, 4517-4527.

[51] Lee, G.; Shin, Y.-H.; Son, J. Y. Formation of Self-Assembled Polyelectrolyte Multilayer Nanodots by Scanning Probe Microscopy. *J. Am. Chem. Soc.* **2009,** *131*, 1634-1635.

[52] Wu, Y.; Shao, B.; Song, Z.; Li, Y.; Zou, Y.; Chen, X.; Di, J.; Song, T.; Wang, Y.; Sun, B. A Hygroscopic Janus Heterojunction for Continuous Moisture-Triggered Electricity Generators. *ACS Appl. Mater. Interfaces* **2022**, *14*, 19569-19578.

For Table of Contents only

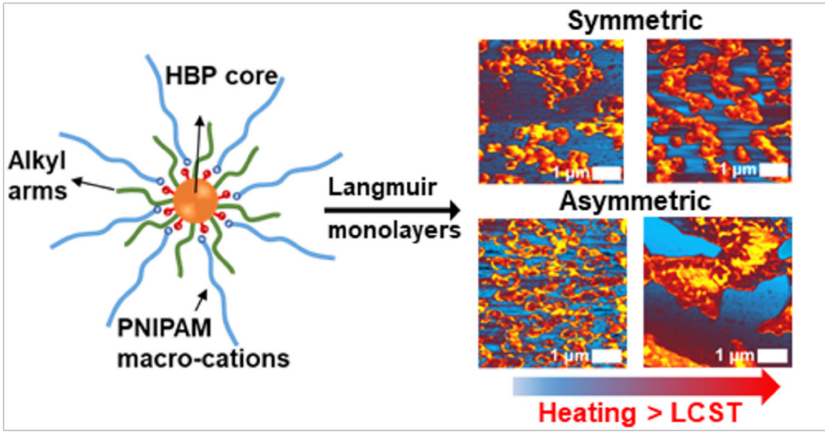

Reversible adsorption and desorption of weakly ionically bound PNIPAM macro-cations to symmetric and asymmetric hyperbranched ionic polymers below and above LCST leads to reorganization of multimolecular micellar assemblies of Langmuir mnolayers with variant surface chemistries